https://ntrs.nasa.gov/search.jsp?R=20110013644 2019-08-30T16:12:12+00:00Z

Development of the Orion Crew Module Static Aerodynamic Database, Part I: Hypersonic

Karen L. Bibb*, Eric L. Walker†
Gregory J. Brauckmann‡
NASA Langley Research Center, Hampton, VA 23681
Philip E. Robinson§
Johnson Space Center, Houston, TX

The Orion aerodynamic database provides force and moment coefficients given the velocity, attitude, configuration, etc. of the Crew Exploration Vehicle (CEV). The database is developed and maintained by the NASA CEV Aerosciences Project team from computational and experimental aerodynamic simulations. The database is used primarily by the Guidance, Navigation, and Control (GNC) team to design vehicle trajectories and assess flight performance. The initial hypersonic re-entry portion of the Crew Module (CM) database was developed in 2006. Updates incorporating additional data and improvements to the database formulation and uncertainty methodologies have been made since then.

This paper details the process used to develop the CM database, including nominal values and uncertainties, for Mach numbers greater than 8 and angles of attack between 140° and 180°. The primary available data are more than 1000 viscous, reacting gas chemistry computational simulations using both the LAURA and DPLR codes, over a range of Mach numbers from 2 to 37 and a range of angles of attack from 147° to 172°. Uncertainties were based on grid convergence, laminar-turbulent solution variations, combined altitude and code-to-code variations, and expected heatshield asymmetry. A radial basis function response surface tool, NEAR-RS, was used to fit the coefficient data smoothly in a velocity–angle-of-attack space. The resulting database is presented and includes some data comparisons and a discussion of the predicted variation of trim angle of attack and lift-to-drag ratio. The database provides a variation in trim angle of attack on the order of ±2°, and a range in lift-to-drag ratio of ±0.035 for typical vehicle flight conditions.

Nomenclature

C_x	A force or moment coefficient
C_A	Axial-force coefficient
C_D	Drag-force coefficient
C_L	Lift-force coefficient
C_m	Pitching-moment coefficient
$C_{m_{apex}}$	C_m, resolved at vehicle theoretical apex
$C_{m_{cg}}$	C_m, resolved at *cg* location
$C_{m_{cgx}}$	C_m, resolved at *mrc* along centerline
C_N	Normal-force coefficient
C_n	Yawing-moment coefficient
cg	Center of gravity
d_2	Bias correction factor for range-based standard deviation
FMV	Blended velocity function
k	Coverage factor, typically $\sqrt{3}$
kfps	kilo-feet per second
L/D	Lift-to-Drag ratio
M_∞	Freestream Mach number
MI	Margin Index
mrc	Moment reference center
$\overline{R_i}$	Range of data for condition i

*Research Engineer, Aerothermodynamics Branch, Senior Member AIAA
†Research Engineer, Configuration Aerodynamics Branch, Senior Member AIAA
‡Research Engineer, Aerothermodynamics Branch, Associate Fellow AIAA
§Aerospace Engineer, EG311 Division

uC_x	Uncertainty in a force or moment coefficient
UF_{C_x}	Database uncertainty factor for a force or moment coefficient
U_∞	Freestream velocity
α	Angle of attack, deg.
α_T	Total angle of attack, deg.
β	Sideslip angle, deg.
ϕ	Roll angle, deg.
δ	Increment or range to cover
σ	Standard deviation

Subscripts

alt	Altitude
grid	CFD grid convergence
hs	Heatshield asymmetry
idat	IDAT backshell angle change
interp	Interpolation
ltp	Laminar-turbulent variations
c2c	CFD code-to-code variations

I. Introduction

The Apollo-derived Orion Crew Exploration Vehicle (CEV) was designed by NASA and its industry partners within the now-cancelled Constellation Program as part of the Agency's Exploration Mission, and was intended to be the foundation for manned exploration of the Moon, Mars, and beyond.[1,2] The Orion CEV design is now the reference vehicle for the development of the Multi-Purpose Crew Vehicle (MPCV), the exploration vehicle that will carry crew to space, provide emergency abort capability, sustain the crew during the space travel, and provide safe re-entry from deep space return velocities.[3,4] The CEV (and now the MPCV) consists of the Crew Module (CM), Service Module, Spacecraft Adapter, and Launch Abort Tower, as shown in Figure 1. The Orion CM is similar in shape to, but larger than the Apollo capsule. A test flight planned for late 2013, designated Orion Flight Test 1 (OFT-1), will focus on the entry phase of flight for the CM.

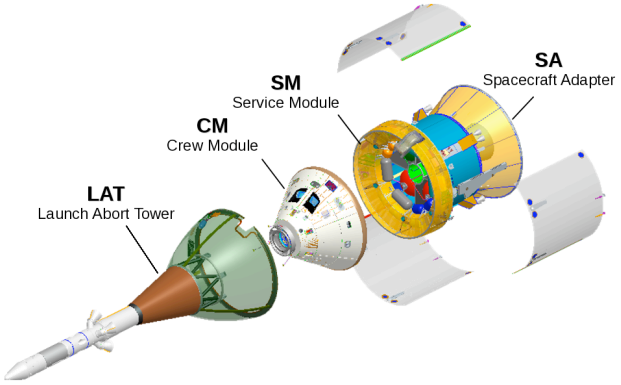

Figure 1: Orion Crew Exploration Vehicle components

The Orion aerodynamic database[5,6] has been developed by the CEV Aerosciences Project (CAP), and is regularly updated with improvements to the aerodynamic modeling of various systems. The primary function of the database is to provide aerodynamic data to the trajectory simulations that are used to develop the guidance, navigation, and control systems for the vehicle and provide targeting and landing ellipse prediction during flight operations. The aerodynamic database development process is shown notionally in Figure 2. Note that this paper will use the term aerodatabase throughout to refer to the Orion aerodynamic database. The CAP team provides this data through an API (Application Programming Interface) that is integrated into the trajectory simulation tools. The API uses tabulated nominal and uncertainty aerodynamic data to compute and return the aerodynamic forces and moments acting on the vehicle at the desired vehicle state. The tabular data is developed from various computational and experimental sources. Uncertainties due to turbulence modeling, grid resolution, wind tunnel repeatability, and other physical modeling are combined to provide tabulated database uncertainties. The CAP database covers the aerodynamics for all phases of the vehicle flight beginning with the separation from the launch system (including nominal and abort situations) until the CM re-enters the atmosphere and lands.

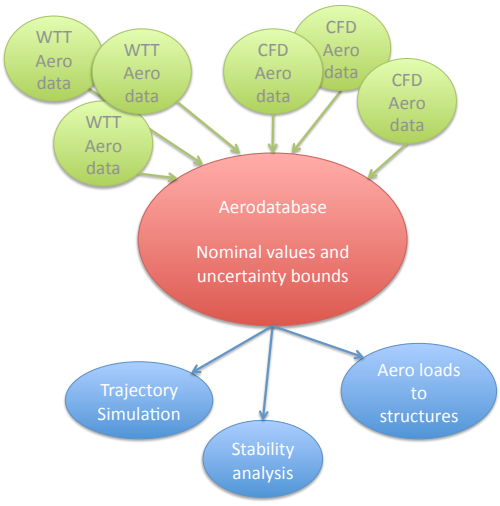

Figure 2: CAP aerodatabase development process.

This paper describes the general process of developing the nominal static aerodynamic coefficients and

uncertainties for the hypersonic flight regime of the Orion Crew Module (CM) and how these are collected into an aerodynamic database for use in the design and development of the CM. The process described reflects the current methodology for the database development, rather than corresponding to a particular database release; some of the analysis shown here has yet to be incorporated into the official database release. This work covers the trim region for the vehicle, $140° \leq \alpha \leq 180°$, for $M > 8$. A companion paper[7] covers the database development for $M \leq 8$.

The available computational hypersonic data, both viscous and inviscid, are discussed, with particular attention paid to comparisons between the various data sets and how well the data covers the expected trajectory space. The basic process for combining the available data into a single response surface, as a function of velocity and total angle of attack is outlined, and the formulation of the uncertainties and development of each term is discussed. Particular attention is paid to the response surface development, effects of altitude variation, and asymmetry effects. The application of the database to determine vehicle trim characteristics is discussed.

II. Database Setup

II.A. Orion Crew Module Geometry

The nominal analytical Orion CM geometry is based on the Apollo configuration, and is shown in Figure 3. The spherical heatshield and conical backshell have been scaled to a maximum diameter of 198 *in* compared to Apollo's 154 *in*. The CEV apex is truncated to accommodate docking hardware.

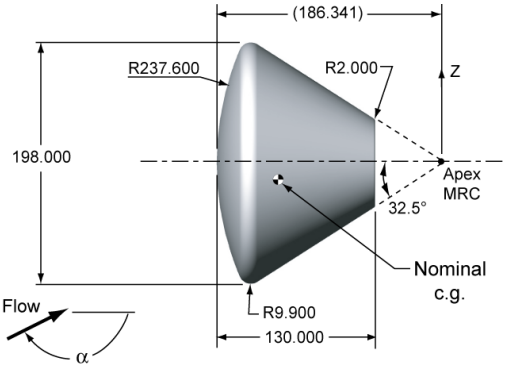

Figure 3: Dimensions of the smooth, axisymmetric baseline Orion Crew Module.

The flight geometry is still being developed, and departs from the nominal, axisymmetric geometry in several key areas. The aerodatabase addresses these geometry differences by incorporating additional analysis to adjust the nominal coefficients and using uncertainties to cover expected variations. The geometry variations fit into three main categories.

First, the nominal 32.5° backshell angle was widened by 2.5° (to 30°), moving the theoretical apex further from the vehicle base, as shown in Figure 4. This modification provides more packaging volume for the parachute system and is referred to as the IDAT geometry[a]. Initial experimental and computational data were generated on the axisymmetric nominal geometry. Subsequent computational studies on the IDAT geometry have been performed, and the effect of incorporating the backshell angle change into the database is covered below.

The second major departure from the nominal geometry was reshaping the heatshield to minimize the thickness of the thermal protection system (TPS), resulting in an asymmetric heatshield shape. Conceptually, the shape is designed to be thicker in the higher heating regions such that the expected ablation drives the shape closer to the nominal spherical shape, and implies that the effect of the asymmetry will be greatest at the highest entry speeds. While this shape is still evolving, there have been some studies to address the aerodynamic effect. The studies have been primarily at hypersonic conditions, and are briefly discussed below in the uncertainty section.

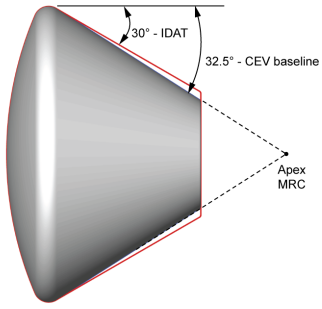

Figure 4: Dimensions of the axisymmetric baseline Orion Crew Module.

The last group of geometry variations include features such as footwells, windows, steps in backshell tile thicknesses, and other protuberances. The aerodynamic effects of these relatively small features have not been quantified, and are assumed to be accounted for within the uncertainty model, as discussed further in the uncertainty section.

[a] The effort to redesign the packaging and deployment schedule for the parachute system was called the Integrated Design Assessment Team, and the resulting changes to the CM vehicle are generically called the IDAT geometry.

II.B. Crew Module Coordinate System Conventions

The CM coordinate system, angle of attack, and aerodynamic coefficient orientation conventions are shown in Figure 5, taken from the CEV Aerodynamic Databook.[5] Note in particular that a heatshield-forward attitude has an angle of attack of 180°.

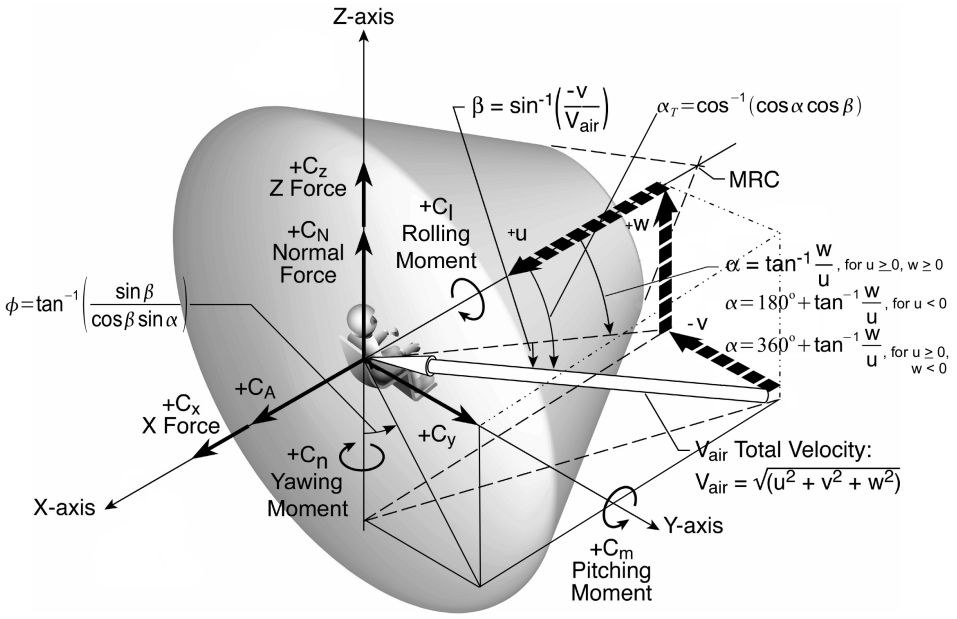

Figure 5: Axis, Force, and Moment Definitions for Crew Module.[5]

The aerodynamic moments are typically resolved about a nominal *cg* location defined by the Orion Project. Through the course of the CM development, the nominal *cg* location has shifted, primarily providing progressively smaller offsets of the *cg* location in the *z-axis* direction. The CAP team typically considers moments resolved about three different *mrc* locations: apex, *cg*, and symmetric *cg*. The database is provided with the moment about the theoretical apex for the nominal, 32.5° backshell, geometry (labeled MRC in Figure 5). The flight *cg* location is used to determine flight characteristics such as trim angle of attack, and is provided as an output of the API. The symmetric *cg* (a location along the *x-axis* corresponding to the *cg* with no *y-* or *z-axis* offsets) is used to develop the nominal pithching-moment coefficient so that symmetry conditions can be enforced. Moment uncertainties are developed for either the *cg* or symmetric *cg* location.

II.C. CM Database Formulation

The CM portion of the database provides the aerodynamic forces and moments as a function of a velocity parameter, FMV, and the orientation of the vehicle with respect to the flow. The database formulation takes advantage of the fact that the vehicle is primarily axisymmetric and treats the nominal coefficients as functions of FMV and α_T only. Tables are provided for C_A, C_N, and C_m, and transformations made to compute the full set of coefficients. The velocity parameter, FMV, is defined in Equation 1 as

$$FMV = \begin{cases} M_\infty & \text{if } U_\infty \leq 8.8\,kfps \\ M_\infty(9.8 - U_\infty) + U_\infty(U_\infty - 8.8) & \text{if } 8.8\,kfps < U_\infty < 9.8\,kfps \\ U_\infty & \text{if } U_\infty \geq 9.8\,kfps, \end{cases} \tag{1}$$

where U_∞ is given in units of *kfps*. The FMV function provides a single velocity parameter for the entire database by taking advantage of the near numerical equivalency of Mach number and velocity (in *kfps*) around Mach 10[b]. The blended parameter provides a smooth transition between Mach number for subsonic and supersonic speeds and velocity for hypersonic speeds.

[b] Note that the formulation of FMV complicates the direct application of the Orion aerodatabase to entry simulations on other bodies, such as Mars.

Because the vehicle is predominately axi-symmetric, the database formulation treats the nominal coefficients as functions of FMV and α_T only. Tables are provided for C_A, C_N, and C_m, and transformations made to compute the full set of nominal coefficients.

The database API computes dispersed aerodynamic coefficients based on the data in the uncertainty tables. In order to facilitate development of dispersed trajectory simulations (typically Monte Carlo based), the user provides an uncertainty factor for each uncertainty coefficient, and the nominal and uncertainty values are combined to form the dispersed coefficient. For a particular simulation within a dispersed trajectory simulation, the user provides an uncertainty factor, typically in the range $-1.0 \leq UF_{C_x} \leq 1.0$, which will be applied to the aerodynamics for that simulation. An uncertainty factor of zero will return the nominal coefficient for C_x, and $UF_{C_x} = 1.0$ will return the nominal plus the total uncertainty for C_x. For the Orion database, all uncertainties are specified as uniform uncertainties except for the rolling moment uncertainty which is treated as a normal distribution. This means that the uncertainty factors chosen for the dispersed trajectory set will be chosen based on a uniform distribution from -1.0 to $+1.0$.

Table 1 specifies the database tables required for the CM static aerodynamics, and lists the independent parameters for each table.

Table 1: Database tables and arguments for the CM static aerodynamics.[6]

Nominal				Uncertainties				
Coefficient	Table Name	Table Arguments		Coefficient	Table Name	Table Arguments		
C_A	CACM	FMV	α_T	uC_D	UCDCM	FMV	α_T	
C_N	CNCM	FMV	α_T	uC_L	UCLCM	FMV	α_T	
				$u(L/D)$	ULODCM	FMV	α_T	
$C_{m_{apex}}$	CMCM	FMV	α_T	$uC_{m_{cg}}$	UCMCGCM	FMV	α	β
				$uC_{n_{cg}}$	UCLNCGCM	FMV	α	β
				$uC_{l_{cgx}}$	UCLLCM	FMV		

Note that the nominal force coefficients are provided as axial and normal force coefficients, but the uncertainties are provided for lift and drag. This is done to allow the dispersed forces to be limited by an uncertainty on L/D[c], and for the convenience of the trajectory simulations (allowing independent evaluation of drag uncertainty in particular). Dynamic coefficients (C_{m_q}, C_{n_r}) and increments due the proximity of other vehicles are not covered herein[d]. The static force coefficients are built from the tabular data and provided uncertainty factors as follows. First, lift and drag uncertainties are extracted from the tables. Note that this process is more complicated if the correlation with L/D is being applied.

$$\texttt{UCD} = \texttt{UFCD} * \texttt{UCDCM}(FMV, \alpha_T) \tag{2}$$

$$\texttt{UCL} = \texttt{UFCL} * \texttt{UCLCM}(FMV, \alpha_T) \tag{3}$$

The force uncertainties are then transformed to the body-axis system,

$$\texttt{UCA} = \texttt{UCD}\cos\alpha\cos\beta - \texttt{UCL}\sin\alpha \tag{4}$$

$$\texttt{UCN} = \texttt{UCD}\sin\alpha\cos\beta + \texttt{UCL}\cos\alpha \tag{5}$$

$$\texttt{UCY} = -\texttt{UCD}\sin\beta \tag{6}$$

The moment uncertainties for pitch and yaw are extracted and uncertainty factors applied as

$$\texttt{UCM} = \texttt{UFCM} * \texttt{UCMCGCM}(FMV, \alpha, \beta) \tag{7}$$

$$\texttt{UCLN} = \texttt{UFCLN} * \texttt{UCLNCGCM}(FMV, \alpha, \beta). \tag{8}$$

[c] This is effectively a correlation. In order to keep the analysis simple, the correlation is not applied in this work

[d] See Owens, *et al.*[8] for details on the dynamic portion of the CM database, and Rhode, *et al.*[9] for proximity increment data.

The remainder of the tabular data is then extracted, and combined with the input uncertainty factors to provide the final, dispersed coefficients. For the force and rolling-moment coefficients, this process is straightforward,

$$C_A = \texttt{CACM}(FMV, \alpha_T) + \texttt{UCA} \quad (9)$$
$$C_Y = -\texttt{CNCM}(FMV, \alpha_T)\sin\phi + \texttt{UCY} \quad (10)$$
$$C_N = \texttt{CNCM}(FMV, \alpha_T)\cos\phi + \texttt{UCN} \quad (11)$$
$$C_l = \texttt{UFCLL} * \texttt{UCLLCM}(FMV). \quad (12)$$
$$(13)$$

For the pitching- and yawing-moment coefficients, the table value is extracted and transformed into the undispersed values at the apex *mrc* location

$$C_{m_{apex}} = \texttt{CMCM}(FMV, \alpha_T)\cos\phi \quad (14)$$
$$C_{m_{apex}} = -\texttt{CMCM}(FMV, \alpha_T)\sin\phi. \quad (15)$$

The undispersed moments are transferred to the desired *mrc* location using undispersed forces and then the uncertainty values from eqns 7 and 8 are added. Note again that only the static portion of the coefficients are developed herein; the full buildup can be found in the Orion Aerodatabase Formulation document.[6]

II.D. Available Computational Data

The hypersonic portion of the CM database is derived entirely from computational data, and is provided as a function of FMV and α_T only[e]. The distribution of data in velocity, angle of attack, and altitude is shown in Figure 6. The primary data is from computations using the viscous, reacting gas CFD codes LAURA[10,11] and DPLR.[12–15] These solution sets cover the range of velocities from $1\,km/s < U_\infty < 11\,km/s$, angles of attack between $147° \le \alpha \le 172°$, and altitude ranges appropriate for each velocity; these sets are collectively referred to as the aerothermal dataset. The primary limitation of the aerothermal dataset is that the angle-of-attack range is limited to a shifting trim angle-of-attack range, $147° \le \alpha \le 172°$. The database is required to cover the full angle-of-attack range, from 0° to 180°, and sideslip angles $-90° \le \beta \le 90°$. To cover this expanded space, an inviscid CFD code, FELISA,[16–18] was used to generate a set of solutions on the axisymmetric nominal geometry at various conditions.

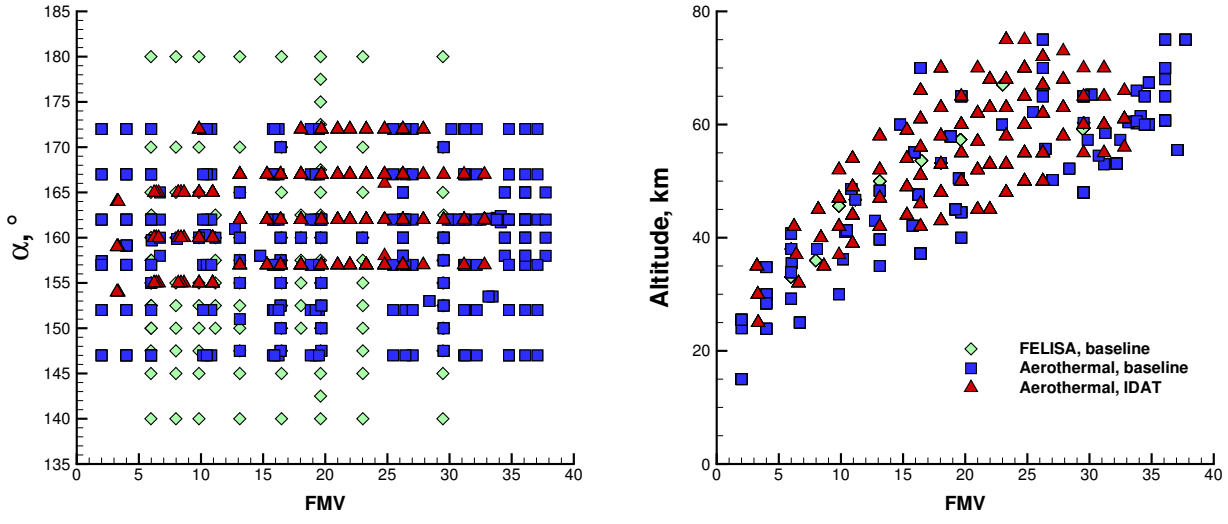

(a) α vs. FMV (b) Altitude vs. FMV

Figure 6: Distribution of available aerothermal and invisicid data as functions of velocity, angle of attack, and altitude.

[e] In general, all data was developed with $\beta = 0$, so that $\alpha = \alpha_T$. For the data presented herein, α is equivalent to α_T unless specifically noted.

The over 1000 aerothermal solutions that make up the database are viscous, both laminar and turbulent, employ either a 5-species or 11-species reacting gas model, and cover both the nominal smooth geometry (∼600 solutions) and wider backshell angle (IDAT) smooth geometry (∼450 solutions). The effects of these variations on the aerodynamic coefficients are discussed in both the nominal coefficient and uncertainty development sections of this paper.

Each of the available CFD solutions was developed using a standard set of simulation guidelines that assured adequate grid resolution and iterative convergence. The simulation guidelines for FELISA[19] were specifically developed to ensure converged aerodynamic coefficients. Mesh adaptation was used to improve the solutions and provide a measure of grid convergence. For the aerothermal solutions, the simulation guidelines[11,15] were developed to ensure adequate resolution of the heating on the heatshield and attached-flow windside portion of the backshell. First, a laminar solution was developed on a half-body geometry (with a symmetry plane). A turbulent solution was then developed, starting from the laminar. For the IDAT geometry, the simulation guidelines were updated to require that the turbulent solutions be computed on a full geometry (no symmetry plane) and utilize unsteady time-stepping. The aerodynamic coefficients are computed from the final flow solutions; no time-averaging over a range of iterations is employed. While the aerothermal simulation guidelines do not specifically address convergence of the aerodynamic coefficients, the requirements for converged heating are considered more stringent.

The aerothermal data covers a range of altitudes for each velocity condition, as shown in Figure 6(b). For the CEV, variations with altitude of the aerodynamic quantities are small, but not negligible. Figure 7 shows the variation of C_A, C_N, and $C_{m_{cg}}$ with altitude, for a particular velocity, angle of attack, flow solver, and geometry combination. Both laminar and turbulent solutions are shown, and a notional representation of the database is given. Since the aerodatabase is a function of only FMV and α_T, all of these data points correspond to a single table value in the database, and their variation is accounted for by an uncertainty term.

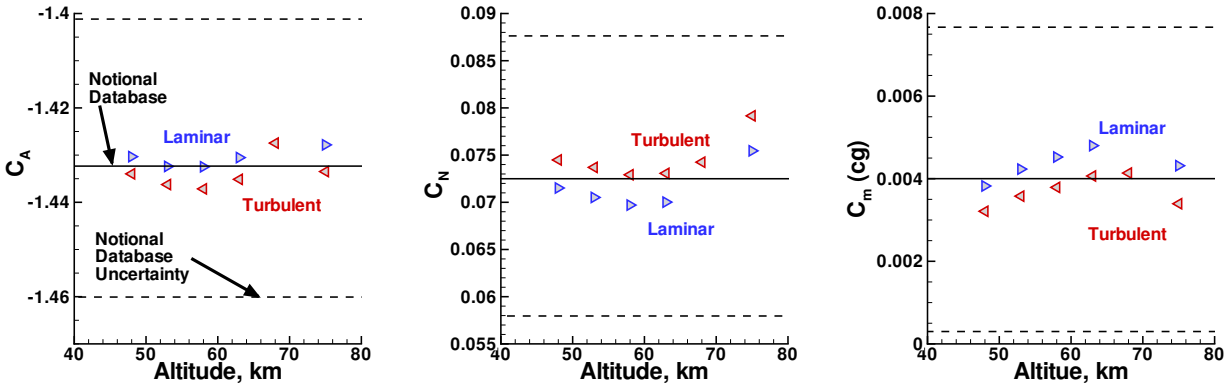

(a) C_A (b) C_N (c) $C_{m_{cg}}$

Figure 7: Typical variation in aerodynamic coefficients for various altitudes.

Figure 7 also shows the difference in the aerodynamic coefficients between the laminar and turbulent flow solutions. In general, it is not known whether a given flow condition will remain laminar over the entire vehicle, or where transition to turbulent flow will occur. As such, we use the average of the laminar and the turbulent solution at a particular condition in the development of the database, and recognize that these two conditions might not fully bound the aerodynamics for the flow condition. The average data points are referred to as the laminar-turbulent pair, *ltp*, data.

Additional data from computations of various asymmetric heatshield shapes were used to incorporate the effects of the designed TPS and expected recession into the aerodatabase. These studies[20,21] were primarily conducted with FELISA, with some anchoring to viscous computations, and are discussed in the uncertainty development section of this work.

III. Nominal Coefficient Development

A response surface model of the nominal aerodynamic coefficients (C_m, C_A, C_N) as functions of FMV and α_T was developed using the software tool `NEAR-RS`.[22–24] The process began by selecting and processing the available aerothermal data. Additional inviscid data and surrogate database data were added around the edges of the data space to provide smooth blending to the other sections of the database. A response surface was then generated and queried at regular intervals to provide the required tables.

III.A. Aerothermal Data Manipulation

As with most curve fitting and response surface generation tools, `NEAR-RS` does not easily handle multiple data points with identical independent variables. This situation occurs in several dimensions in the aerothermal dataset. For a given value of FMV and α_T, there could be points with different solvers (LAURA and DPLR), laminar and turbulent, and solutions at multiple altitudes. These data must be processed to provide a single value before being input to the response surface tool, and the data variations analyzed to be included in the uncertainty model.

III.A.1. Laminar-Turbulent Pair Data

The first steps in the pre-processing are to remove the solutions where $FMV < 8$ and then average pairs of laminar and turbulent data. This collapses the aerothermal solution set to ∼440 laminar-turbulent-pair (*ltp*) data points. Figure 8 shows the laminar and turbulent aerodynamic coefficients for a single velocity, altitude, and code plotted over a typical angle-of-attack sweep. The increment in the aerodynamic coefficients between laminar and turbulent solutions is fairly consistent and so we simply average the two values and provide a standard deviation to the uncertainty buildup. This does lead to the elimination of solutions where there are not both laminar and turbulent solutions, but this is a small portion of the dataset (about 35 solutions).

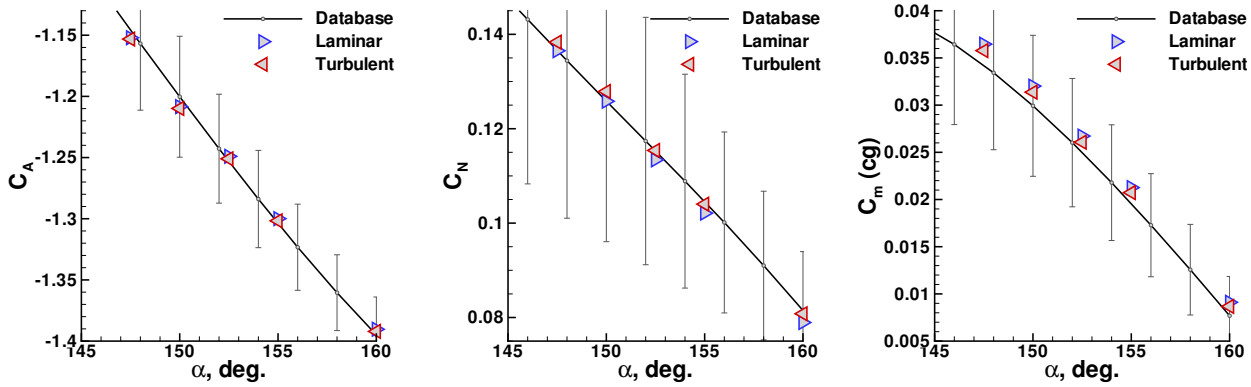

(a) C_A (b) C_N (c) C_N

Figure 8: Typical variation in aerodynamic coefficients between laminar and turbulent aerothermal computations.

III.A.2. Collapsing Data Points

Once the data were averaged into laminar-turbulent pairs, the *ltp* data were further collapsed to a single value for a given (FMV, α_T) combination. Depending on the data space, this could involve solutions at multiple altitudes, geometries, and codes. The available data was generated over several years using multiple CFD codes, with an evolving geometry and shifting trajectory requirements (which led to different angle-of-attack ranges for studies). This situation leads to an inability to easily separate the effects of altitude, code, and geometry. The practical implication is that, for the development of the response surface, all of the *ltp* data for a single (FMV, α_T) combination is averaged. For the current aerothermal data, this results in a final set of about 225 points that range from $8 < FMV < 37$ and $147^\circ < \alpha \leq 172^\circ$.

Figure 9 illustrates the data collapsing process for a representative set of data over several of the angles of attack at a particular velocity. Nominal geometry solutions are shown with the blue symbols. For $\alpha = 157.5°, 160°$, solutions were computed with DPLR for conditions at a low altitude, and with LAURA at a high altitude. For the IDAT backshell geometry (red), solutions where computed with both LAURA and DPLR at multiple altitudes and $\alpha = 157°, 162°$. Note that none of these solutions directly overlap. Lack of overlap is typical and makes distinguishing variation with the independent parameters difficult.

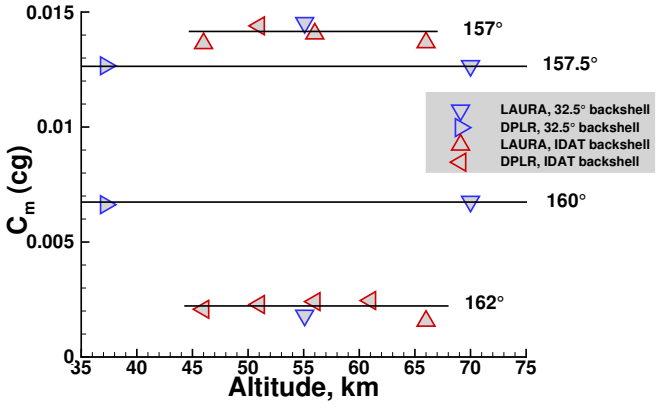

Figure 9: *LTP* data points to collapse over range of altitudes for a specific velocity and several angles of attack

This process is not ideal, as the altitude distribution of the available data can skew the averaging process. For the example shown in Figure 9, the pitching moment is greatest in the middle of the altitude range for α=157°, 162°. Since there are no middle altitude solutions available for the α=157.5°, 160° sets, the average for these angles of attack could be skewed. An alternate methodology would be to recast the altitude variation to a rectangular space, and then develop the response surface with the altitude parameter as a 3rd dimension. The response surface could then be queried either in the middle of the altitude space, or averaged across the altitude dimension. This alternate method may be implemented in the future.

III.A.3. Data for Response Surface Edges

Once the primary data has been collapsed as described above, additional data must be incorporated to ensure that the *FMV*-α_T space is bounded appropriately and blends with the rest of the database. The distribution of the data used for the response is shown in Figure 10, and the various strategies used to anchor the edges of the *FMV*-α_T space are discussed below.

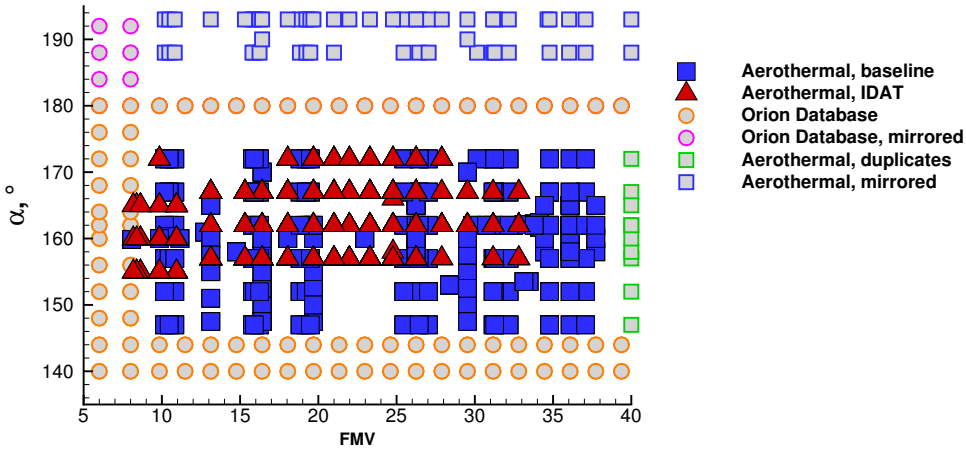

Figure 10: Final data for response surface development.

The early releases of the Orion aerodynamic database were developed using the FELISA inviscid solutions, which covered the full *FMV*-α_T space, and limited aerothermal solutions where available. Rather than use the original FELISA data in the current development, the earlier database was used as a surrogate, as shown by the orange circles in Figure 10. This choice provided a more uniform point distribution and more rigorous blending on the edges connected to other sections of the database across the $FMV = 8$ and $\alpha_T = 140°$ edges. The database is also used along the $\alpha_T = 180°$ edge, helping to enforce the symmetry conditions of $C_L,\ C_{m_{cgx}} = 0$.

To cover the upper edge of the FMV range, the current aerothermal data were extended by copying all aerothermal data for $FMV \geq 37$ and setting $FMV = 40$ for the duplicated points, shown by the green square symbols. Finally, data (both CFD and surrogate database) were mirrored across $\alpha_T = 180°$ to provide for appropriate derivatives across $\alpha_T = 180°$.

III.B. Response Surface Development

Once the input data for the response surface tool has been developed, the `NEAR-RS` tool is fairly simple to use. The primary parameter that must be set is the stiffness of the system. The stiffness controls how well data points are captured. A low stiffness (∼0.01) forces the data points to the surface, causing irregular curves. A higher stiffness produces smoother curves, which are more appropriate for general usage. The stiffness parameter is set to 1.0 for the Orion database development. There are various parameters that control automatic data collapsing and random elimination data points; for the CEV database, they are left at the default values. After the response surface model is generated, the model is queried at the desired breakpoints for the aerodatabase. A final post-processing step enforces symmetry conditions.

Figure 11 shows a 3-dimensional view of the response surfaces generated for each of the primary aerodynamic coefficients, with the input data included. Note that C_L, C_D and $C_{m_{cgx}}$ are developed; these results are converted to C_A, C_N, and $C_{m_{apex}}$ for the database tables. More detailed comparisons are given in the Results section, and include the uncertainty development.

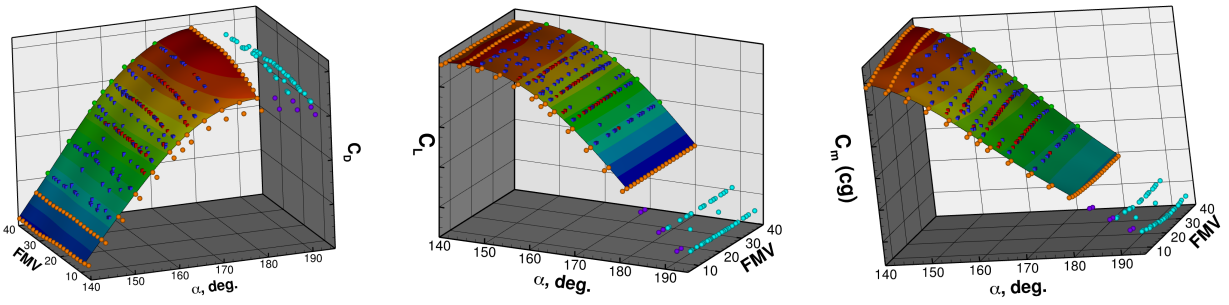

(a) C_D (b) C_L (c) C_m

Figure 11: Response surfaces for aerodynamic coefficients as developed with `NEAR-RS` and compared to the data input to `NEAR-RS`.

IV. Uncertainty Development

The uncertainty buildup follows the general methodology being employed by CAP.[25–30] Individual contributions are developed using accepted statistical and engineering approaches, and then they are combined with either a root sum square (RSS) or additive method. Equation 16,

$$uC_x = \delta_{hs} + MI\sqrt{(k\sigma_{grid})^2 + (k\sigma_{ltp})^2 + (k\sigma_{alt})^2 + (k\sigma_{c2c})^2 + (k\sigma_{idat})^2 + (k\sigma_{interp})^2} \tag{16}$$

is the starting point for the development of the hypersonic uncertainties and represents possible contributions to the uncertainty model for the aerodynamic coefficients. Variations due to heatshield asymmetry are given by δ_{hs}. Grid convergence and iterative solution convergence are accounted by σ_{grid}. The variation between the laminar and turbulent data at each flow condition is represented by σ_{ltp}. Variations due to the altitude range are given by σ_{alt}. The σ_{c2c} term represents the inherent differences in the models and numerics of the different flow solvers used. The altitude and code-to-code variations can be combined as σ_{ks}, so that Equation 16 reduces to

$$uC_x = \delta_{hs} + MI\sqrt{(k\sigma_{grid})^2 + (k\sigma_{ltp})^2 + (k\sigma_{ks})^2 + (k\sigma_{idat})^2 + (k\sigma_{interp})^2} \tag{17}$$

The differences due to the change in backshell angles are covered by σ_{idat}. A term for interpolation error is included in the initial list of contributing uncertainties for completeness; it is set to zero for the final uncertainty buildup. The margin index, (MI), accounts for unknown unknowns, and other desired multipliers.

The standard coverage factor for a uniform uncertainty distribution is given as $k = \sqrt{3}$. The following sections will describe the development of each term, and the adjustments made to Equation 16 in the final buildup.

IV.A. CFD Accuracy Variation, σ_{grid}

The uncertainty term for the accuracy of a particular CFD solution is dominated by a grid convergence term, developed from early solutions on multiple meshes. The uncertainty values, given in Table 2, were developed by differencing solutions on coarse and fine meshes rather than a more standard Richardson extrapolation approach. A more recent examination of a set of meshes for a single flow condition yielded uncertainties ranging from 50%-80% smaller. Terms for unsteadiness and for differences in chemistry model (5- 11 species) were examined, but found to be small in comparison to the (original) grid convergence term. The original uncertainties have been maintained in the buildup in order to maintain some conservatism and, more importantly, because the σ_{grid} term is small in the overall buildup.

Table 2: Grid uncertainty for hypersonic aerothermal CFD solutions.

	C_L	C_D	$C_{m_{apex}}$	$C_{m_{cg}}$	L/D
σ_{grid}	0.0004	0.002	0.0009	0.0023	0.0009

IV.B. Laminar-Turbulent Variation, σ_{ltp}

The variation of the laminar-turbulent pair data is the most straightforward term to compute, and it serves as an example of the standard practice for developing a variational term that is used throughout the Orion aerodatabase development.

The first step is to compute an individual deviation for each coefficient at each *ltp* data point. Since there are many subgroups with a small number of data points in each, a range-based formula,

$$\sigma_i = \overline{R_i}/d_2, \tag{18}$$

is employed to compute the standard deviation for each point, where d_2 is a bias correction factor for converting range to standard deviation based on sample size.[27] For the individual *ltp* data points, where there are only 2 values, the equation becomes

$$\sigma_{ltp_i} = \frac{|C_{x_{turb}} - C_{x_{lam}}|}{d_2}, \tag{19}$$

where $d_2 = 1.128$. Figure 12 shows the approximately 450 individual σ_{ltp_i} values and their average, $\overline{\sigma}_{ltp}$, plotted vs. both FMV and α, for C_D.

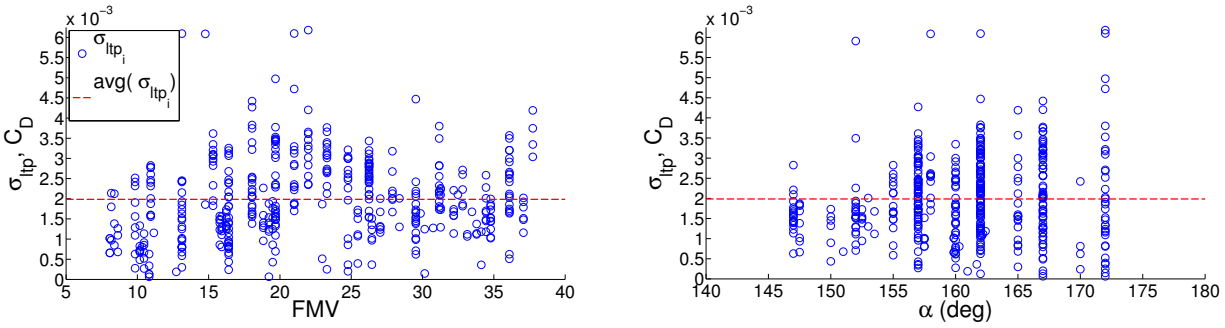

(a) vs. FMV (b) vs. α

Figure 12: *LTP* variation in C_D, σ_{ltp_i}.

From the individual variation terms, the model for the buildup is developed. The model, σ_{ltp}, can be a function of database independent parameters such as FMV and α_T if there is a trend to support this, or it

can be a simple average of all σ_{ltp_i} over the data range. To determine a suitable model for σ_{ltp}, the individual σ_{ltp_i} are plotted vs. both FMV and α, to determine if a reasonable trend exists. To determine if the model for σ_{ltp} is adequate, $k\sigma_{ltp}$ must cover most of the data points. Figure 13 repeats the data from Figure 12, and adds the final values for the modeled σ_{ltp} and the coverage level, $k\sigma_{ltp}$. There is not a clear trend in either FMV or α for C_D, so the model for σ_{ltp} is simply a constant. Note that σ_{ltp} was adjusted higher than $\overline{\sigma}_{ltp}$, so that the coverage was adequate. An alternate, equivalent choice would be to set $\sigma_{ltp} = \overline{\sigma}_{ltp}$ and adjust k higher than the standard value of $k = \sqrt{3}$.

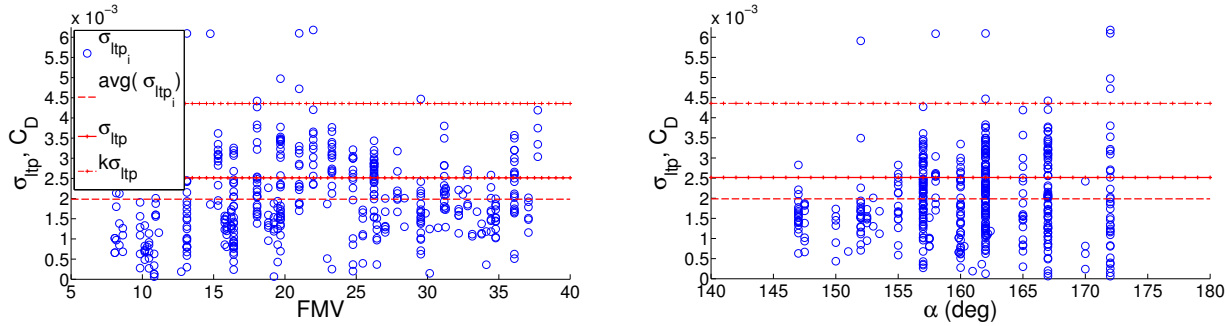

(a) vs. FMV (b) vs. α

Figure 13: Model for σ_{ltp} for C_D, with σ_{ltp_i} and $\overline{\sigma}_{ltp}$.

For C_L, there is a trend in α for σ_{ltp}, with the variation increasing for $FMV > 30$. The model reflects this trend by adding a linear increase in σ_{ltp} for the range $30 < FMV < 40$, as seen in Figure 14

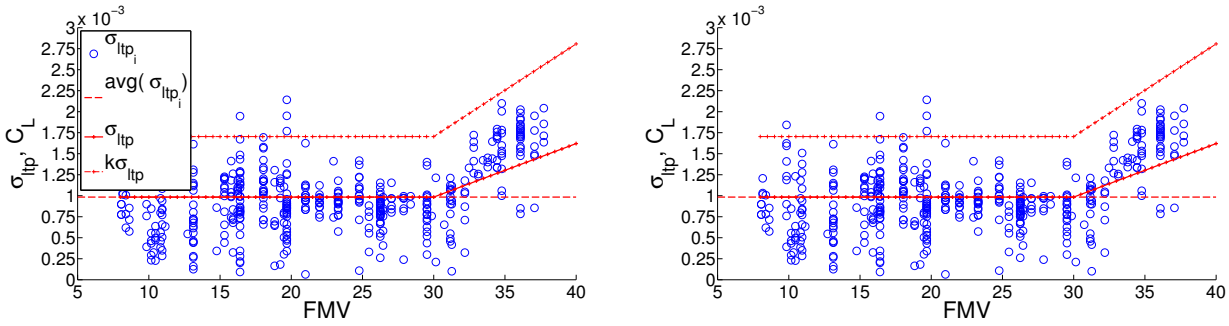

(a) vs. FMV (b) vs. α

Figure 14: Model for σ_{ltp} for C_L, with σ_{ltp_i} and $\overline{\sigma}_{ltp}$.

The final models for σ_{ltp} are shown in the 3-D plots in Figure 15 for each coefficient. The individual σ_{ltp_i} points are shown by the blue (32.5° backshell) and red (IDAT) points. The lower surface represents the model for σ_{ltp}, while the upper surface is $k\,\sigma_{ltp}$. Note that the upper surface covers almost all data points. The uncertainties due to laminar-turbulent variations are modeled as constants for C_m and C_D, and linear in FMV for C_L.

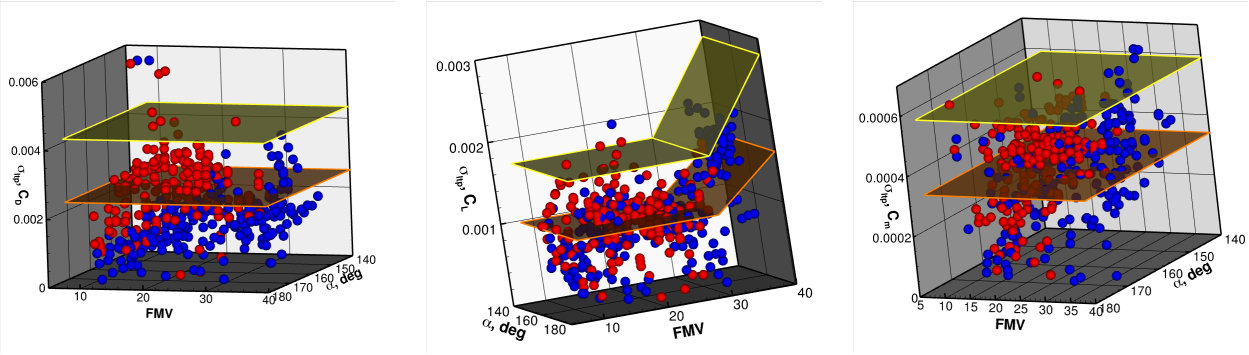

(a) C_D (b) C_L (c) $C_{m_{cgx}}$

Figure 15: Modeled σ_{ltp} variation for all coefficients, lower surface, with coverage of data shown by upper surface, $k\sigma_{ltp}$. Baseline geometry σ_{ltp_i} data plotted as blue spheres and IDAT points are red.

IV.C. Altitude, Code-to-code, and Combined Variations

In the current implementation of the Orion Aerodatabase uncertainty buildup, the variations in the aerodynamic coefficients from altitude variations and differences in CFD codes are treated as a single, lumped term. Early in the program, there was insufficient overlap in both LAURA and DPLR cases to explicitly separate the effects of code and altitude variation. Recent analysis with the current, larger aerothermal data set shows that there is little difference in the results when the terms are lumped or when they are separated and appropriate correlation corrections applied. This section will cover the development of the lumped uncertainty term, σ_{ks}, altitude variation term σ_{alt}, and code-to-code variation term σ_{c2c}. The applicability of utilizing a correlation model to separate the code-to-code and altitude variations is assessed. Note that the final uncertainty buildup uses the lumped, σ_{ks} formulation.

IV.C.1. Combined Altitude and Code-to-code Variation, $\boldsymbol{\sigma}_{\mathrm{ks}}$

The uncertainty term that combines the altitude and code-to-code variations in the aerothermal CFD data was developed in the same manner as described for the σ_{ltp} term that is based on Eqn. 18. All solutions that were at the same velocity and angle of attack were collected and a standard deviation computed for each of nearly 100 *FMV*-α_T points as

$$\sigma_{ks_i} = \frac{|C_{x_{alt_{max}}} - C_{x_{alt_{min}}}|}{d_2}, \tag{20}$$

where d_2 now varies with the number of solutions in the collection.[f] The σ_{ks_i} values were then plotted vs. both *FMV* and α_T to determine trends. The data for $C_{m_{cgx}}$, given in Figure 16, shows σ_{ks} levels decreasing as α_T approaches 180°. This trend is consistent with the physics in that less (absolute) variation would be expected because $C_{m_{cgx}}$ (and C_L) approaches zero as α approaches 180°. Therefore, σ_{ks} is modeled as shown in Figure 16(b).

The variation for C_L shows trends in both *FMV* and α which are captured in a bi-linear model for σ_{ks}. The trends and model are similar to $C_{m_{cgx}}$ for C_D. The final σ_{ks} models for each coefficient are shown in Figure 17.

IV.C.2. Separated Altitude and Code-to-code Variations, $\boldsymbol{\sigma}_{\mathrm{alt}}$ and $\boldsymbol{\sigma}_{c2c}$

An effort was made to account for the altitude and code-to-code variations separately. The σ_{alt_i} values are computed for each group of solutions at the same velocity, angle of attack, and solver. There are approximately 170 sets of σ_{alt_i} data, and these are shown with the mean values for C_D, C_L, and $C_{m_{cgx}}$ plotted vs. *FMV* in Figure 18. Similarly, approximately 40 σ_{c2c_i} values are computed for solutions with different flow solvers at the same velocity, angle of attack, and altitude conditions and shown in Figure 19.

The relative magnitudes of the means of the combined uncertainty, $\overline{\sigma}_{ks}$, compared to the *RSS* of the individual uncertainties, $\sqrt{(\overline{\sigma}_{alt})^2 + (\overline{\sigma}_{c2c})^2}$, suggests that separate uncertainties would overpredict the total

[f] $d_2 = [1, 1.128, 1.693, 2.059, 2.326]$ for $n = [1, 2, 3, 4, 5]$, Ref. 27

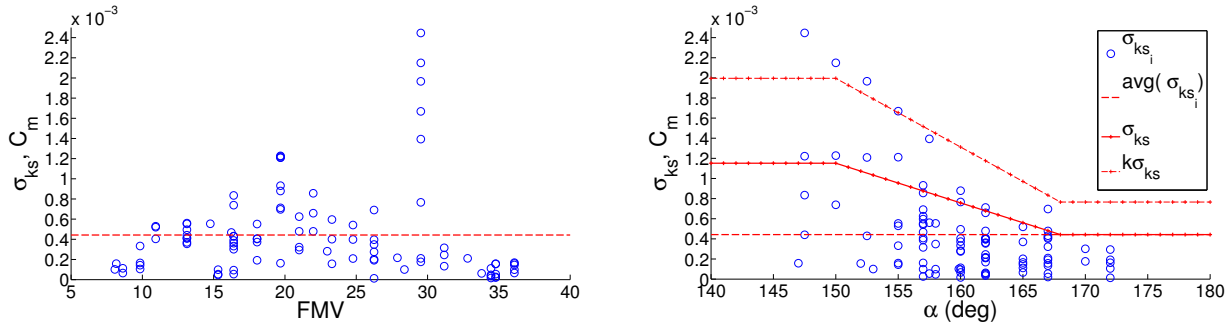

(a) vs. FMV (b) vs. α

Figure 16: Variation in σ_{ks} for $C_{m_{cgx}}$ coefficients.

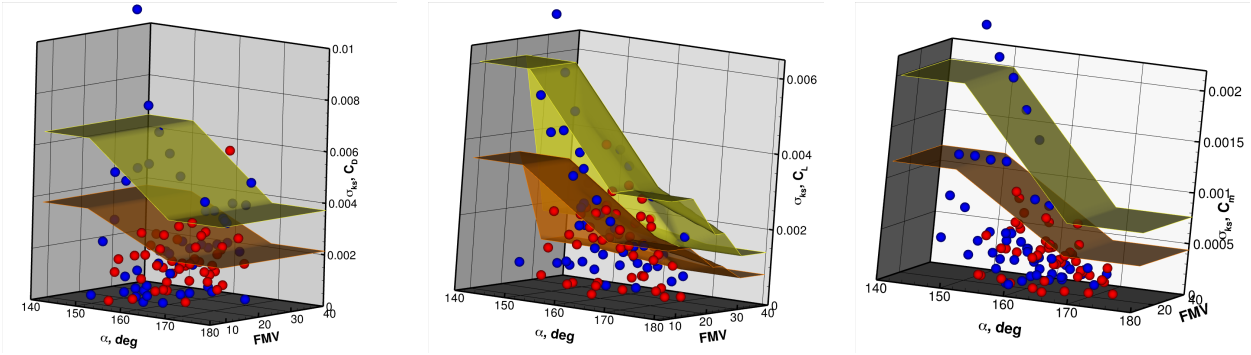

(a) C_D, vs. FMV (b) C_L, vs. FMV (c) $C_{m_{cgx}}$, vs. FMV

Figure 17: Model for σ_{ks} for all coefficients (lower surface), with distinction between backshell geometries shown as blue for baseline and red for IDAT. Final coverage shown by upper surface, $k\sigma_{ks}$.

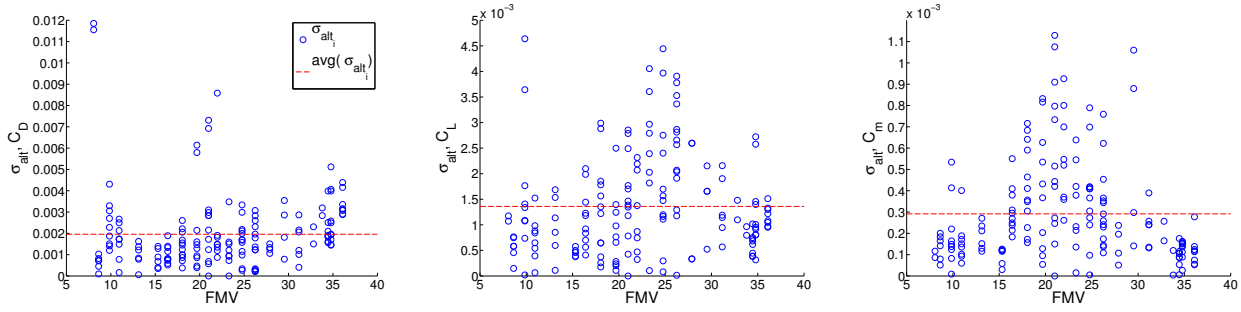

(a) C_D variation (b) C_L variation (c) $C_{m_{cgx}}$ variation

Figure 18: Variation in σ_{alt} for all coefficients, vs. FMV.

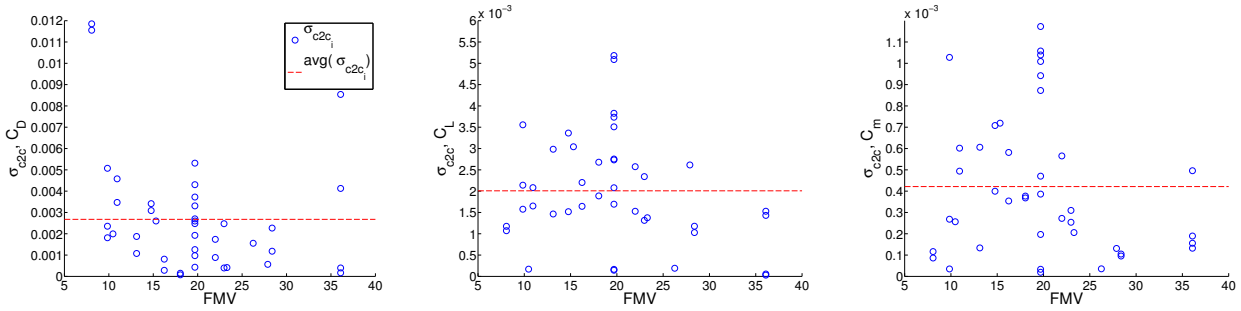

(a) C_D variation (b) C_L variation (c) $C_{m_{cgx}}$ variation

Figure 19: Variation in σ_{c2c} for all coefficients, vs. *FMV*.

variation. Table 3 shows the relative values of the mean variations for each coefficient. Note that the *RSS* value is larger than the corresponding value from the combined analysis, suggesting that there is a correlation between the altitude effects and the code-to-code variation of the solutions. This correlation could arise due to slight differences in how each code handles some aspect of the physics modeling. The methodology developed by Hemsch and Walker[31] was employed to determine the level of correlation, but due to the small set of data, the results were called into question. The original methodology of developing combined uncertainties was retained. As more data becomes available, this analysis will be revisited. Additionally, designing computational studies to provide the appropriate data to compute the correlations properly should be pursued.

Table 3: Combined and separate uncertainties due to altitude and code-to-code variations.

Coefficient	$\overline{\sigma}_{alt}$	$\overline{\sigma}_{c2c}$	$\sqrt{(\overline{\sigma}_{alt})^2 + (\overline{\sigma}_{c2c})^2}$	$\overline{\sigma}_{ks}$
C_D	0.0020	0.0027	0.0034	0.0022
C_L	0.0014	0.0020	0.0025	0.0018
$C_{m_{cgx}}$	0.0003	0.00042	0.00052	0.00045

IV.D. Backshell Angle Variation, σ_{idat}

Quanititatively determining the effect of backshell angle change on the vehicle aerodynamics was not possible because of a lack of overlapping data between the two sets. Instead, data that was nearby was examined graphically, and the differences were negligible. An example graphical comparison between the data for the two geometries is given in Figure 20. Here, DPLR solutions on the baseline geometry are compared to LAURA solutions on the IDAT geometry at an altitude that differs by only $0.5\,km$. The available angles-of-attack overlap and the agreement between the two curves is very good.

While determining a statistical difference in the nominals between the backshell angles was not possible, it was noticed that the *ltp* variation in C_D was noticeably higher for the IDAT backshell, as seen in Figure 15(a). The small difference may be because of the increased area of the backshell region for the IDAT geometry.

IV.E. Interpolation Error, σ_{interp}

Defining a model for interpolation error proved problematic. The response surface tool, `NEAR-RS`, outputs a confidence-interval type estimate for the surface fit uncertainty, which is sensitive to the stiffness parameter. The results of this type of uncertainty estimate tend to be very small when the stiffness of the response surface model is high. A more appropriate measure of uncertainty would be a prediction-interval type estimate, which was unavailable with the `NEAR-RS` tool. An alternate method of evaluating the difference between the response surface output and a data point that wasn't included in the initial development is also problematic, due to the variations (such as altitude) that are covered by the database with the uncertainty

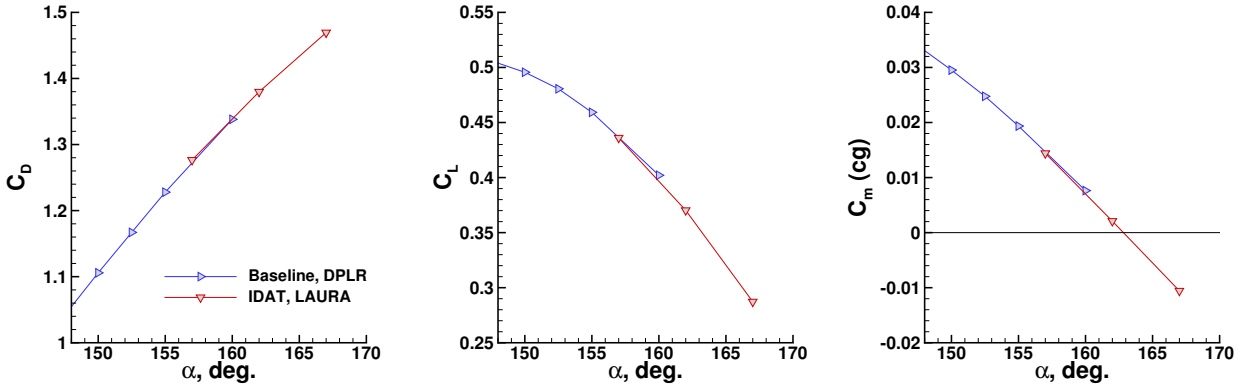

(a) C_D (b) C_L (c) $C_{m_{cg}}$

Figure 20: Overlap between aerodynamic coefficients for baseline and IDAT configurations, showing no quantifiable difference.

model. Becuase of these difficulties, the interpolation error is ignored in the uncertainty buildup, such that

$$\sigma_{interp} \approx 0. \tag{21}$$

Properly utilizing updated capability within `NEAR-RS` to provide interpolation error estimates will be explored in the future.

IV.F. Uncertainty Buildup for RSS Combined Term

Once the uncertainties for each contributing term were modeled, the terms were combined at each point in the FMV-α_T space covered by the database for the RSS portion of the model and is given by:

$$RSS = \sqrt{(k\sigma_{grid})^2 + (k\sigma_{ltp})^2 + (k\sigma_{ks})^2}. \tag{22}$$

Note that the σ_{idat} and σ_{interp} terms have been eliminated from Equation 16, and that the σ_{alt} and σ_{c2c} are replaced by σ_{ks}. Figure 21 shows a sample of the buildup for the final RSS term. In general, the σ_{ks} term dominates, with the σ_{ltp} term more important in some areas. Figure 22 shows the same terms over the full FMV-α_T space.

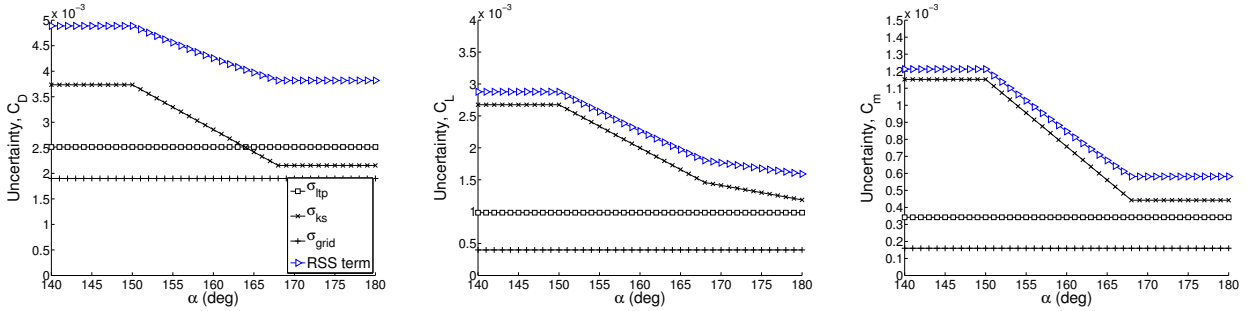

(a) C_D (b) C_L (c) $C_{m_{cg}}$

Figure 21: Buildup of the RSS portion of the uncertainty term for a specific Mach number over the angle-of-attack range.

IV.G. Heatshield Asymmetry Uncertainty Increment, δ_{hs}

The heatshield shape for the CEV is not finalized as of the time of this writing. The heatshield is being designed with a variable thickness across the entire shape to minimize weight while still providing the necessary thermal protection. The recession model for the heatshield also has large uncertainties, although

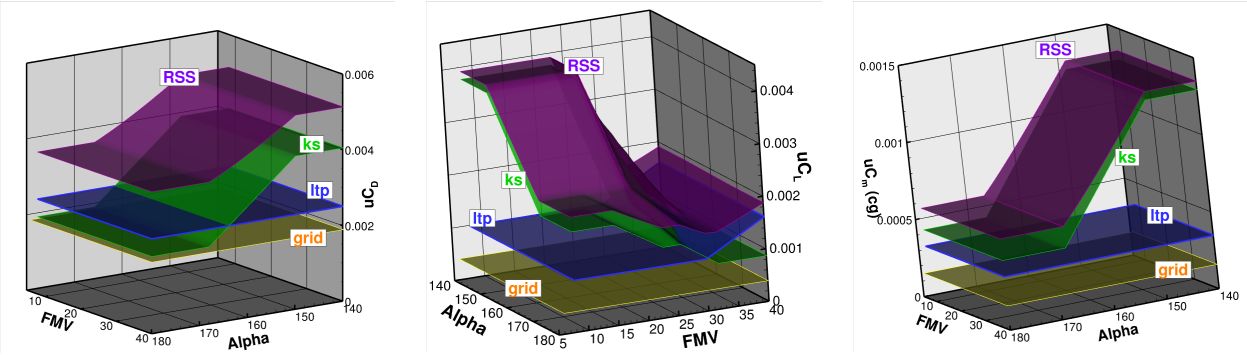

(a) C_D (b) C_L (c) $C_{m_{cg}}$

Figure 22: Buildup of the *RSS* portion of the uncertainty term.

minimal recession is expected for LEO entry conditions. As such, expected variations in heatshield shape are accounted for in the uncertainties for the aerodynamic database.

To quantify the effects of changes in heatshield shapes, various shapes have been compared to the baseline. The bulk of the analysis has been performed with the inviscid tool, FELISA, and documented in Refs. 20, 21. The shapes analyzed have been snapshots of the vehicle geometry at different times in the design process. The most recent geometry analyzed for an ISS return trajectory is considered to be the most representative of the current design. In all of these studies, increments in the aerodynamic coefficients were computed at various velocities and angles of attack. Overall, the increments are predominantly a function of shape. The increments are virtually independent of velocity (at least for the hypersonic velocities considered) and show only small trends with angle of attack for most of the geometries. Figure 23 shows the increments in the aerodynamic coefficients for a collection of heatshield shapes, and the uncertainties that have been defined based on these increments.

The first set of geometries (square symbols) came from an early recession study,[20] where the heatshield was initially axisymmetric. The recession model for the initial TPS material[g] produced an asymmetric geometry with the thickest region opposite from the stagnation point. The predicted maximum recession for the final (130) geometry was much larger than current recession predictions; the earliest geometry (013) had a maximum recession of 0.5in, which is more consistent with models for recession levels for lunar trajectories with the current heatshield material, Avcoat. These geometries show little differences in the force coefficients. The pitching moment increment is increasingly negative as the TPS recesses; this trend is expected to hold for the current recession model. Additionally, a few points were computed with LAURA and DPLR, and the results support using the invicid code, FELISA, for computing heatshield aerodynamic increments.

The second set of geometries, designated PICA Rev I and Avcoat Rev J, were designed to optimize the TPS thickness distribution for a lunar return trajectory such that the heatshield was thickest near the stagnation region and would recess toward a more axisymmetric shape. These shapes provided a comparison of optimized geometries for each of the two TPS materials, and were the basis of a detailed CAP study.[21] The PICA geometry showed a large increase in drag primarily because the TPS thickness around the shoulder resulted in a projected heatshield area much larger than the other geometries considered. Avcoat is less ablative than PICA, and was used for the original Apollo capsule.[2,32] The tailored geometry for Avcoat was more asymmetric than the PICA heatshield, and as such showed a larger variation in pitching moment. Note that the program chose Avcoat for the TPS, and so the PICA increments are not relevant to the uncertainties except they show how C_D increases as the overall vehicle diameter increases.

The final set of geometries, designated Rev Q, were generated to compare optimized heatshields for a lunar and an ISS return trajectory. Of course, the lunar heatshield required significantly more TPS material around the stagnation region, and thus was more asymmetric than the ISS-optimized heatshield; the lower increment in C_m is a direct result of the smaller level of asymmetry. The differences in C_L between the Rev Q Lunar and the Avcoat Rev J arise from differences in the shoulder rather than the spherical dish region. The Rev Q ISS geometry is closest to the current design, and as such, the uncertainties must cover these increments.

[g] Phenolic Impregnated Carbon Ablator, PICA

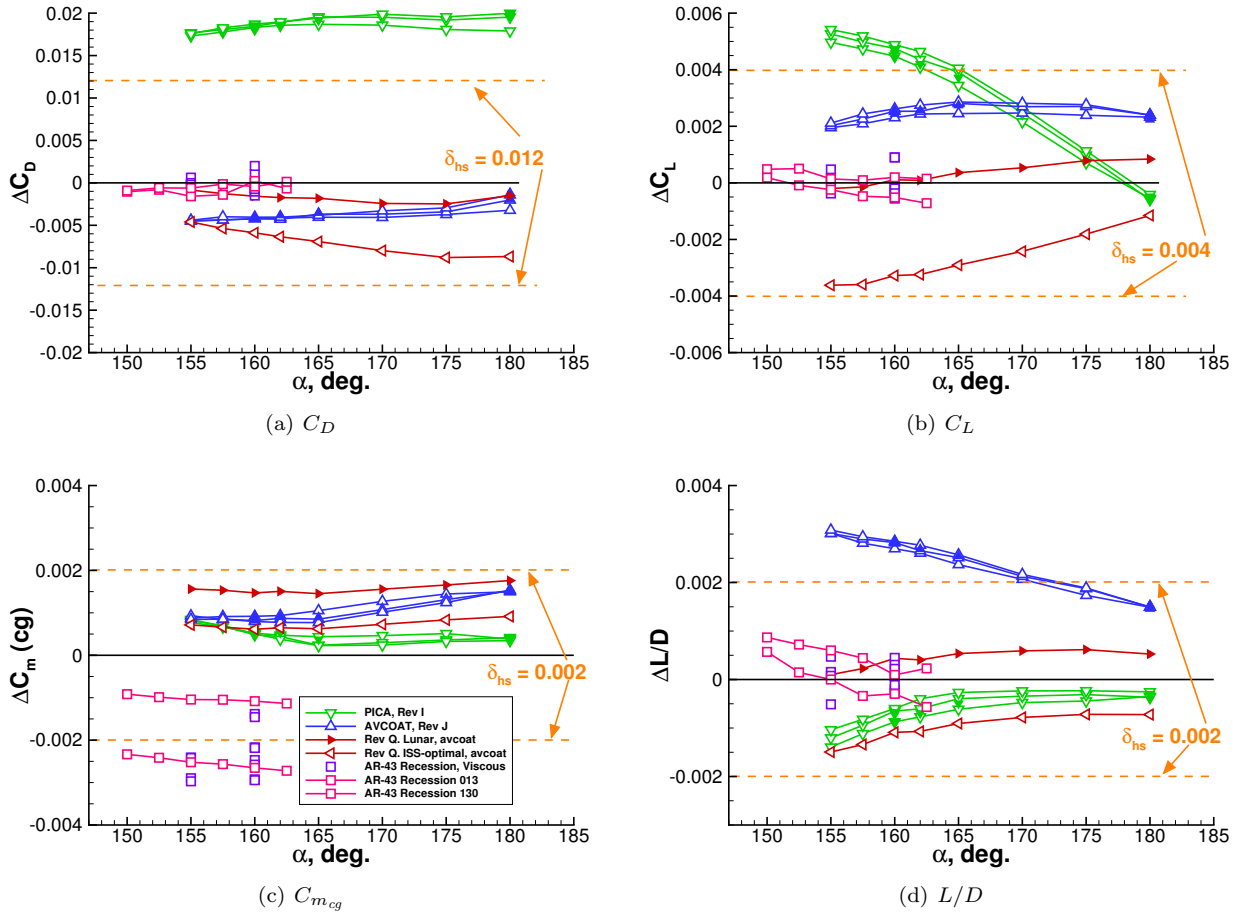

(a) C_D (b) C_L

(c) $C_{m_{cg}}$ (d) L/D

Figure 23: Coverage for asymmetric heatshield shape

Figure 23 includes an uncertainty band for each coefficient. This band was set by visually examining the data, rather than by a rigorous mathematical process. The bands cover the most relevant data and are forced to be symmetric. For C_D and C_L, the PICA data is ignored, and the band covers the primary Rev Q ISS data. The coverage for L/D is set to $\delta_{hs} = 0.002$. This value does not cover the majority of the Avcoat Rev J data, but it is assumed that C_L (and therefore L/D) are larger because of an unrealistic shoulder geometry. For C_m, the highly recessed geometries, which are asymmetrically recessed in an opposite direction from the current design, are ignored, while the maximum level is set to cover the geometries designed for lunar return. It is anticipated that with better analysis of the current ISS and OFT-1 trajectories, this increment could be reduced. For the current database, an increment of in pitching moment of 0.002 represents about a 0.7° change in the trim angle of attack.

IV.H. Final Uncertainty Buildup, Longitudinal Coefficients

The final buildup for the longitudinal coefficient uncertainties is given as

$$uC_x = \delta_{hs} + M\!I\sqrt{(k\sigma_{grid})^2 + (k\sigma_{ltp})^2 + (k\sigma_{ks})^2}, \tag{23}$$

where $M\!I$ is set to 2.0, $k = \sqrt{3}$ for all terms, and the individual terms are developed as above. The choice for $M\!I = 2.0$ was made before the current IDAT data was available; and it will be lowered in future database releases. Figure 24 and 25 show the final uncertainty model for each of the longitudinal coefficients with the relative magnitudes of the asymmetry contribution and the RSS term. Figure 24 shows the model for a specific FMV value over the angle of attack range. The two terms both contribute, with the RSS term more dominate for the lower angles of attack. The RSS term is largely irreducible because it is dominated by the

altitude and laminar-turbulent coverage terms. Reducing the uncertainties due to the heatshield asymmetry will be possible once the heatshield design is finalized. Additional analysis of the final heatshield design will allow the nominal coefficients to be centered on the asymmetric shape, and the uncertainties will be reduced by only needing to cover ablation effects.

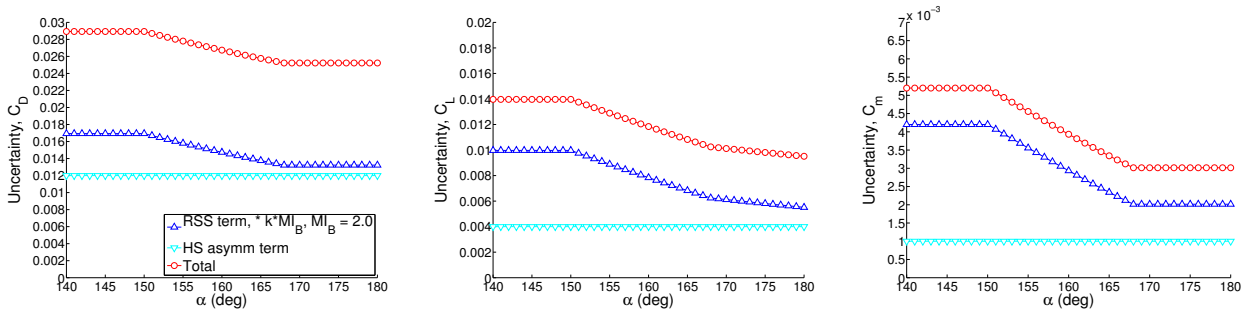

(a) C_D (b) C_L (c) $C_{m_{cg}}$

Figure 24: Buildup of the final uncertainty term for a specific Mach number over the angle-of-attack range.

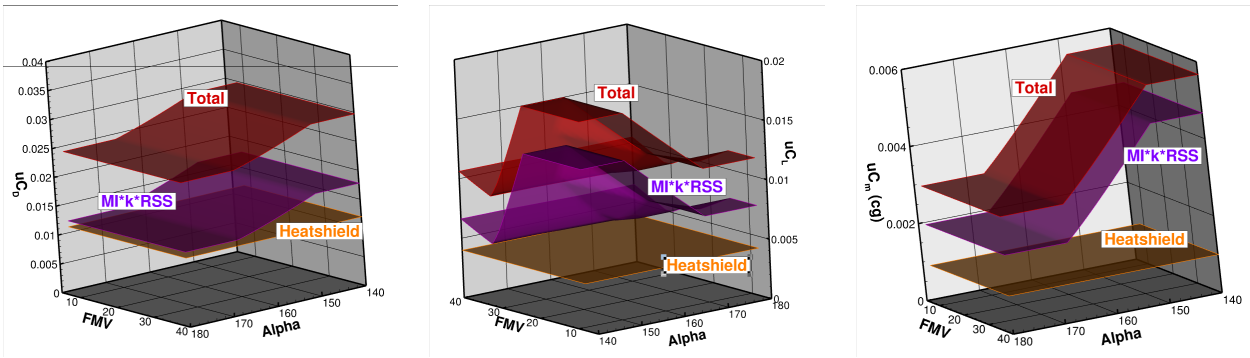

(a) uC_D (b) uC_L (c) $uC_{m_{cgx}}$

Figure 25: Buildup of the full of the uncertainty term, with the heatshield asymmetry term and $MI = 2.0$

IV.I. Lateral-directional Uncertainties

The nominal and uncertainty development presented thus far has focused on the longitudinal aerodynamic coefficients. In reality, there is some finite level of uncertainty in the lateral-directional coefficients (C_y , C_n, and C_l). Developing these uncertainties is a challenge, as the majority of analysis is done for $\beta = 0°$ where these coefficients are either zero (for compuatational analyses), or smaller than balance uncertainties (in experimental data).

Formulation of the yawing-moment uncertainties, based on the pitching-moment uncertainties in α_T, has undergone several iterations in the CAP database process and currently requires developing tables for uC_m and uC_n as functions of (FMV, α, β). The simple transformation used to develop the tables that are currently in the hypersonic CM database CM database is limited in several ways, and can only be considered reasonable in the trim region where β is small ($\pm 5°$) and $\alpha_T < 175°$. An improved approach to transforming $uC_m(\alpha_T)$ to $uC_m(\alpha, \beta)$ and $uC_n(\alpha, \beta)$ has been developed and applied to the database for $M \leq 8$, and is briefly discussed in the companion paper describing the database development for $M \leq 8$.[7]

Side-force uncertainty is computed as

$$uC_Y = -uC_D \sin \beta, \tag{24}$$

with the unfortunate consequence of $uC_Y = 0$ when $\beta = 0°$. Rolling moment uncertainties have been set to a nominal value of $C_l = 0.00005$ everywhere.

The formulation for all of the lateral-directional uncertainties is still a work in progress, with no results shown here. As data for the asymmetric vehicle at small sideslip angles becomes available, the formulations for the lateral-directional coefficients will be revisited.

V. Results

V.A. Final Comparisons of Database Nominals and Uncertainties to Available Data

Figure 26 shows a typical set of plots of the aerodatabase data with uncertainties compared to the available CFD data. As expected, the data variation is captured by the uncertainties. Comparisons are similar across the Mach number range.

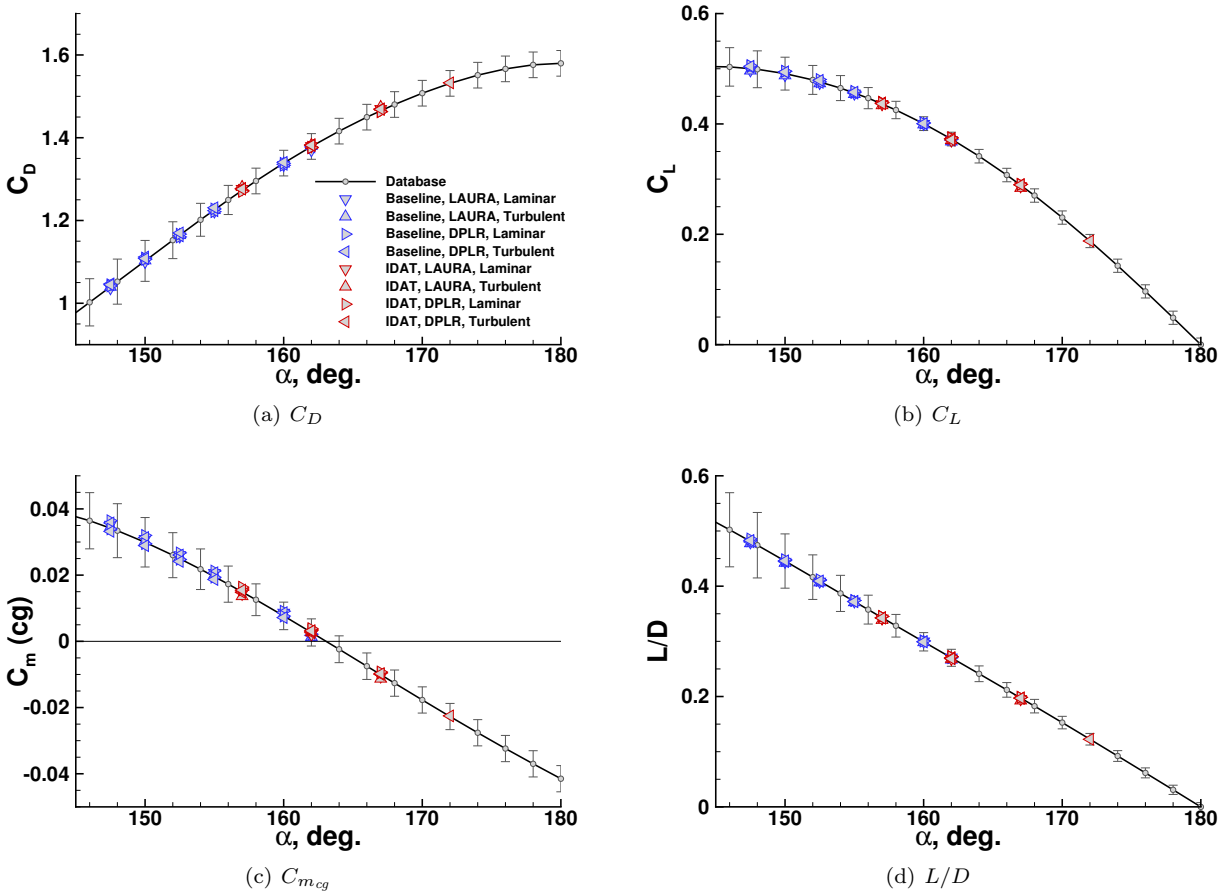

(a) C_D (b) C_L

(c) $C_{m_{cg}}$ (d) L/D

Figure 26: Database with uncertainties compared to available data, for a particular *FMV*.

V.B. Trim Angle and L/D Comparisons

For the hypersonic portion of the entry, the primary performance measure is L/D. This parameter determines available cross-range and down-range capability, and correlates with GNC metrics of target misses, etc. The variation in L/D is a function of both the uncertainties in C_D and C_L at a particular angle of attack[h], as well as the uncertainty in the angle of attack being flown. The trim angle of attack is defined as where the pitching moment is zero, and thus depends on the uncertainty in the pitching moment about the vehicle *cg* and, in turn, the uncertainty in the vehicle *cg* location. To explore the uncertainties, the Orion aerodatabase was queried with various uncertainty factors applied to the relevant coefficents (as described in Eqns. 9-15) and the results examined in the following series of plots.

[h] or the uncertainty in L/D when the L/D correlation function is being applied

Figure 27 shows L/D at the trim angle across the FMV range. The symbols represent the uncertainty band for L/D developed from applying the database table values for UCDCM and UCLCM[i] with uncertainty factors of $UFC_L, UFC_D = [-1, 0, 1]$. Note that the uncertainties are not symmetric about the nominal L/D; this is expected when both uC_L and uC_D are varied uniformly. Utilizing the clipping with the L/D uncertainty would force the variation to be symmetric about the nominal.

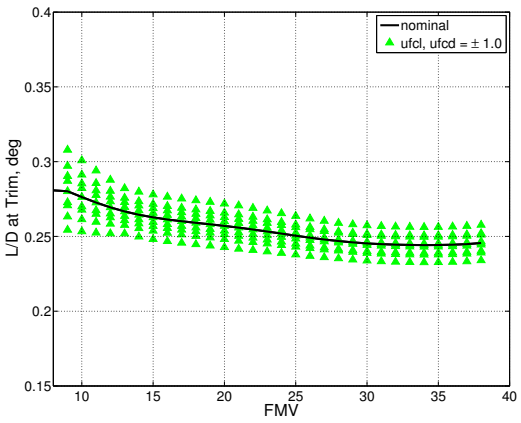

Figure 27: L/D at trim angle of attack, with variations from uC_D and uC_D.

Next, the uncertainty for pitching moment is applied, with $UFC_m = [-1, 0, 1]$. Figure 28(a) shows a plot of trim angle-of-attack vs. FMV for the pitching moment at a nominal cg location, with the symbols indicating the maximum and minimum trim angles for a single cg location. The corresponding range in L/D is also shown, with the various colored symbols representing the range with the full uncertainties in lift and drag applied. With the maximum aerodynamic uncertainties applied, pitching moment about a nominal cg location varies between $\pm 1.5°$ to $\pm 2.0°$, and the L/D range is approximately ± 0.035.

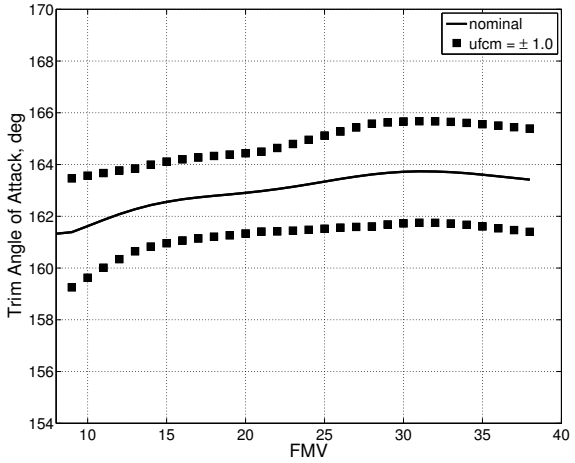

(a) Trim angle of attack for nominal $C_{m_{cg}}$

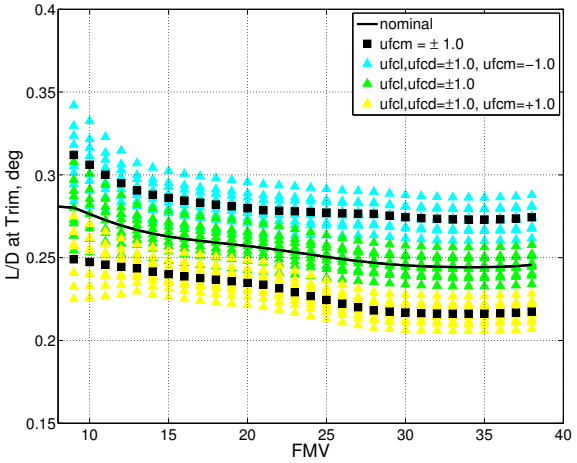

(b) L/D

Figure 28: Nominal and dispersed α_{trim} and L/D, lift, and drag, with uncertainties in C_L, C_D, and $C_{m_{cg}}$ applied.

Finally, the z-cg location is varied, and the resulting trim angles of attack and L/D at trim plotted in Figure 29. Figure 29(a) shows that the uncertainties in z-cg result in approximately the same level of trim angle change as uC_m, and therefore doubles the full trim angle range to approximately $\pm 3°$. This range of trim angle variation results in a range for L/D of approximately ± 0.05. Variations that would yield trim angles with $\beta \neq 0°$ were not included.

[i] when the L/D correlation function is, applied the table values for UCDCM and UCLCM are adjusted based on C_L, C_D, and UCLODCM.

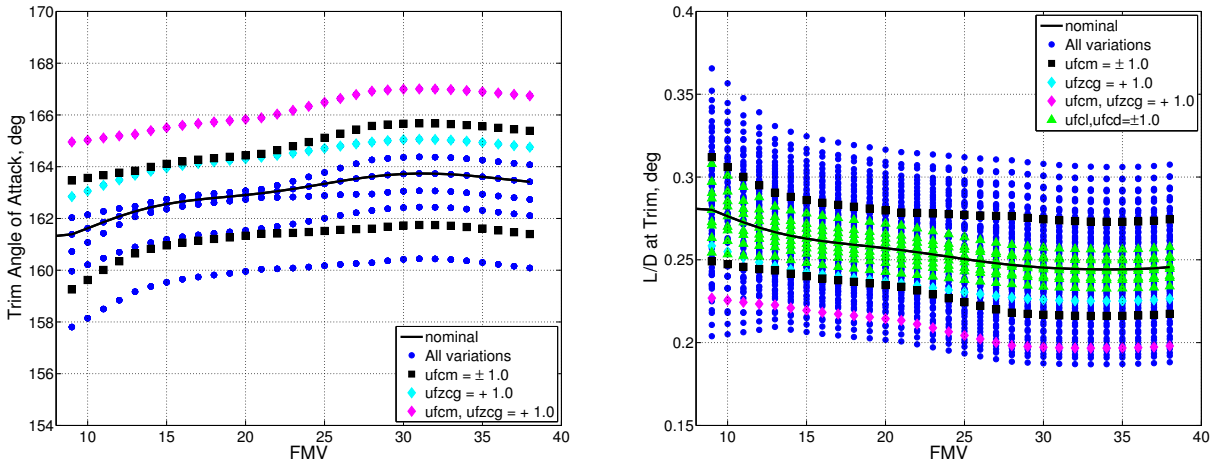

(a) Trim angle of attack

(b) L/D

Figure 29: Nominal and dispersed α_{trim} and L/D, lift, and drag, with uncertainties in cg location, C_L, C_D, and $C_{m_{cg}}$ applied.

VI. Concluding Remarks

The development of the static aerodynamic database for the CEV Crew Module for the trimmed hypersonic flight regime covering $8 < FMV < 40$ and $140° < \alpha < 180°$ has been presented. The database development is based primarily on CFD computations performed with the LAURA and DPLR codes over a large range of altitudes and velocities in the trim angle-of-attack range. Outside of the trim range, an earlier release of the database is used on the edges of the angle-of-attack and FMV ranges, and thus FELISA inviscid CFD solutions are implicitly included. A response surface, with independent parameters FMV and α_T, has been developed from the available data to provide the nominal coefficients (C_A, C_N, C_m) for the database. Uncertainties are quantified for individual viscous solution uncertainty (primarily grid convergence), laminar-turbulent variations, combined code-to-code and altitude variations, and heatshield asymmetries. The margin index is intended to cover unknown and un-quantified but recognized unknowns including response surface interpolation errors and flight test/prediction comparisons. The various contributions to the uncertainties are combined to provide database tables for uC_D, uC_L, $u(L/D)$, uC_m, and uC_n with independent parameters of FMV and α_T (or α, β).

The Orion aerodynamic database is used by other disciplines in the design process for the CEV. Quantities such as hypersonic L/D ratio are key parameters to ensure landing accuracy. The database provides a variation in trim angle of attack on the order of $\pm 2°$, and a range in L/D of ± 0.035.

The data presented here does not correspond directly to a particular implementation of the Orion aerodatabase. Rather, the methodologies and comparisons presented are representative of those used in the database development, but utilize data not yet incorporated into the database.

Acknowledgments

The authors would like to acknowledge the efforts of the CAP Aerothermal Team for developing the LAURA and DPLR computational data used in the hypersonic aerodatabase development. Particular thanks are due to Grant Palmer (Ames Research Center, Aerothermal Smooth Body OML Working Group) for coordinating development and delivery of the aerodynamic data from the Smooth Body OML WG, and Rick Thompson (Langley Research Center, Aerothermodynamics Branch) and Vic Lessard (Langley Research Center, Aerothermodynamics Branch) for their assistance and diligence in reviewing the aerodynamic results. The authors would also like to thank Jeremy Rea (Johnson Space Center, GNC Entry Abort Mode Team Lead) and Tim Crull (Johnson Space Center, GNC Entry Abort Mode Team) for many conversations about the impact of the aerodynamic database uncertainties on the entry trajectory simulations.

References

[1]NASA, http://www.nasa.gov/mission_pages/constellation/orion/, last accessed 05 June 2011.

[2]NASA, "Orion Next Generation Spacecraft," http://www.nasa.gov/pdf/491544main_orion_book_web.pdf, last accessed 05 June 2011.

[3]NASA, http://www.nasa.gov/exploration/systems/mpcv/, last accessed 05 June 2011.

[4]NASA, "Preliminary Report Regarding NASAs Space Launch System and Multi-Purpose Crew Vehicle," http://www.nasa.gov/pdf/510449main_SLS_MPCV_90-day_Report.pdf, January 2011, last accessed 05 June 2011.

[5]CAP Aerodynamics Team, "Orion Aerodynamic Databook, Version 0.60.0, Volume 1," NASA CXP-72167, January 2011.

[6]CAP Aerodynamics Team, "Formulation of the Orion Aerodynamic Database," CEV Aerosciences Project EG-CEV-06-37, Rev. 0.60.0, Rev. 1, NASA Johnson Space Center, Houston, TX, October 2009.

[7]Bibb, K. L., Walker, E. L., Brauckmann, G. J., and Robinson, P. E., "Development of the Orion Crew Module Static Aerodynamic Database, Part II: Supersonic/Subsonic," 29th AIAA Applied Aerodynamics Conference, Honolulu, HI, 27-30 June 2011, American Institute of Aeronautics and Astronautics, Reston, VA (submitted for publication).

[8]Owens, D. B. and Aubuchon, V. V., "Overview of Orion Crew Module and Launch Abort Vehicle Dynamic Stability," 29th AIAA Applied Aerodynamics Conference, Honolulu, HI, 27-30 June 2011, American Institute of Aeronautics and Astronautics, Reston, VA (submitted for publication).

[9]Rhode, M. N., Chan, D. T., Niskey, C. J., and Wilson, T. M., "Aerodynamic Testing of the Orion Launch Abort Tower Separation with Jettison Motor Jet Interactions," 29th AIAA Applied Aerodynamics Conference, Honolulu, HI, 27-30 June 2011, American Institute of Aeronautics and Astronautics, Reston, VA (submitted for publication).

[10]Mazaheri, A., Gnoffo, P. A., Johnson, C. O., and Kleb, B., "LAURA Users Manual: 5.3-48528," NASA TM 2010-216836, August 2010.

[11]Zoby, E. V., Pulsonetti, M., Alter, S., Thompson, R., Meyers, B., Greene, F., Lessard, V., Weilmeunster, J., Hollis, B., and Jentink, T., "Guidelines for Application of the LAURA code for CEV," CEV Aerosciences Project EG-CEV-07-53, 2007, Langley Research Center.

[12]Candler, G. V., Wright, M. J., and McDonald, J. D., "Data–Parallel Lower–Upper Relaxation Method for Reacting Flows," *AIAA Journal*, Vol. 32, No. 12, 1994, pp. 2380–2386.

[13]Wright, M. J. and Candler, G. V., "The Solution of the Navier-Stokes Equations Using Gauss-Seidel Line Relaxation," *Computers and Fluids*, Vol. 17, No. 1, pp. 135–150.

[14]Wright, M. J., Candler, G. V., and Bose, D., "Data–Parallel Line Relaxation Method for the Navier–Stokes Equations," *AIAA Journal*, Vol. 36, No. 9, 1998, pp. 1603–1609.

[15]McDaniel, R., Brown, J., Tang, C., Olejniczak, J., Bahram, P., Dateo, C., Liu, Y., Yoon, S., and Palmer, G., "Best Practices for DPLR CEV Aerothermal Database Solutions, v2," CEV Aerosciences Project EG-CAP-07-167, version 2.0, 2007, Ames Research Center.

[16]Peiro, J., Peraire, J., and Morgan, K., "FELISA Reference Manual and User's Guide, Volume I," University of Wales/Swansea Report CR/821/94, 1994.

[17]Bibb, K. L., Peraire, J., and Riley, C. J., "Hypersonic Flow Computations on Unstructured Meshes," AIAA Paper 97-0625, January 1997.

[18]Bibb, K. L., Gnoffo, P. A., Park, M. A., and Jones, W. T., "Parallel, Gradient Based, Anisotropic Mesh Adaptation for Re-entry Vehicle Configurations," AIAA Paper 2006–3579, June 2006.

[19]Bibb, K. L., "CEV CFD Simulation Guidelines for the FELISA Solver," CEV Aerosciences Project EG-CEV-06-30, 0.9.2 release, 2006, Langley Research Center.

[20]Bibb, K. L., Alter, S. J., and McDaniel, R., "Aerodynamic Analysis of Simulated Heat Shield Recession for the Orion Crew Module," AIAA Paper 2008–0356, January 2008, Presented at the 2008 AIAA Aerosciences Meeting and Exhibit.

[21]Bibb, K. L., "Assessment of CM including asymmetric heatshield effects," CEV Aerosciences Project EG-CEV-08-142, NASA Langley Research Center, Hampton, VA, 2009, CAP-AR-95.

[22]Rodman, L. C., Reisenthel, P. H., and Childs, R. E., "An Automated Documentation and Reporting System For CFD," AIAA Paper 2002–0986, January 2002, Nielsen Engineering & Research, Mountain View, CA.

[23]Reisenthel, P. H., Love, J. F., Leiseutre, D. J., and Childs, R. E., "Cumulative Global Metamodels with Uncertainty: a Tool for Aerospace Integration," Tech. Rep. CEIAT 2005-0019, August 2005, Presented at the 1st International Conference on Innovation and Integration in Aerospace Sciences, Queens University Belfast, Northern Ireland, UK, 4-5 August 2005.

[24]Nielsen Engineering & Research, Mountain View, C., "Multidimensional Response Surface Package: NEAR RS," http://www.nearinc.com/index.cfm?fuseaction=page.display&page_id=90, last accessed 19 April 2011.

[25]"U.S. Guide to the Expression of Uncertainty in Measurement," Tech. Rep. ANSI/NCSL Z540-2-1997, October 1997.

[26]Wheeler, D. and Chambers, D., *Understanding Statistical Process Control, 2nd ed.*, SPC Press, Knoxville, 1992.

[27]Wheeler, D., *Advanced Topics in Statistical Process Control*, SPC Press, Knoxville, 1995.

[28]Wheeler, D., *Range Based Analysis of Means*, SPC Press, Knoxville, 2003.

[29]Harter, H., "Tables of Range and Studentized Range," *The Annals of Mathematical Statistics*, Vol. 31, No. 4, December 1960, pp. 1122–1147.

[30]Hemsch, M. J., Tuttle, D., Houlden, H., and Graham, A., "Measurement of Force Balance Repeatability and Reproducibility in the NTF," AIAA Paper 2004-0771, January 2004.

[31]Hemsch, M. J. and Walker, E. L., "The Crucial Role of Error Correlation for Uncertainty Modeling of CFD-Based Aero Increments," AIAA Paper AIAA-2011-173, January 2011.

[32]Strouhal, G., Curry, D. M., and Posgay, R. G., "Definition of Entry Corridor Thermal Limits for Apollo Spacecraft," AIAA Paper 68–1144, December 1968.